Intermetallics. Vol. 15. Núm. 10. 2007. Pag. 1351-1360
http://dx.doi.org/10.1016/j.intermet.2007.04.008

Nanocrystalline Fe-Nb-(B,Ge) alloys from ball milling: Microstructure, thermal stability and magnetic properties

J. S. Blázquez, V. Franco, C.F. Conde, A. Conde*

Dpto. Física de la Materia Condensada, ICMSE-CSIC, Universidad de Sevilla, P.O. Box 1065, 41080, Sevilla, Spain

Keywords: mechanical milling, nanocrystalline microstructure, magnetic properties

Abstract

$Fe_{75}B_{20}Nb_5$, $Fe_{75}Ge_{10}B_{10}Nb_5$ and $Fe_{75}Ge_{20}Nb_5$ alloys were prepared by ball milling from pure powders and their microstructure and magnetic properties were studied. A nanocrystalline solid solution of α-Fe type is the main phase formed, although traces of some intermetallics were found in the Fe-B-Nb alloy. The local arrangements of Fe atoms in Ge containing alloys continuosly evolves with milling time. The obtained powders are thermally stable even heating up to 773 K. After heating up to 1073 K, intermetallic compounds are detected. The best soft magnetic properties are achieved after heating up to 773 K, due to stress relaxation of the nanocrystalline microstructure (for Fe-Ge-Nb alloy, coercivity ~600 A/m).

*Corresponding author: Prof. A. Conde

Departamento de Física de la Materia Condensada. Universidad de Sevilla.

Apartado 1065, 41080 Sevilla (Spain).

Phone: (34) 95 455 28 85

Fax: (34) 95 461 20 97

E-mail: conde@us.es

Intermetallics. Vol. 15. Núm. 10. 2007. Pag. 1351-1360
http://dx.doi.org/10.1016/j.intermet.2007.04.008

1. Introduction

A strong development of soft magnetic materials occurred after the discovery of nanocrystalline FINEMET alloys in 1988 [1]. Since then, big effort has been devoted to improve their technological capabilities and to understand the interactions appearing in the biphasic microstructure (~10 nm nanocrystals embedded in a residual amorphous matrix) responsible for their outstanding soft magnetic behaviour [2].

Nanocrystalline microstructure is generally achieved by partial crystallization of a precursor amorphous alloy obtained by rapid quenching techniques (PCPA). This implies several restrictions concerning the size of the samples (generally ribbons of a few tens of microns thick) and the available compositions (close to deep eutectics). Besides this, the nanocrystallization of amorphous ribbons yields brittle materials [3]. Mechanical alloying (MA) has shown to be a low-cost and very versatile technique in order to produce metastable microstructures: amorphous, nanocrystalline, quasicrystalline, extended solid solutions and metastable intermetallics [4]. Unlike nanocrystalline materials obtained from devitrification of amorphous precursors, MA would overcome the restrictions of small compositional ranges and final size by powder compaction. However, soft magnetic properties of MA nanocrystalline samples are clearly worse than those exhibited by samples obtained from PCPA [5] (coercivity of ~1-10 kA/m and ~10 A/m, respectively). However, low coercivity values (25 A/m, comparable to those of ribbon shaped samples) have been recently reported for mechanically alloyed bulk amorphous compositions after compaction and annealing [6].

Amorphous compositions close to the deep eutectic of the binary Fe-B system have been widely studied. The addition of an early transition metal, ET, (Zr, Nb, Hf, etc) to this system leads to NANOPERM-type alloys, which develop a nanocrystalline microstructure during their primary crystallization process [7]. In these alloys, the

Intermetallics. Vol. 15. Núm. 10. 2007. Pag. 1351-1360
http://dx.doi.org/10.1016/j.intermet.2007.04.008

growth of the α-Fe phase is constrained to the nanometer size as the ET, insoluble in the nanocrystals, piles up at the edge of the nanocrystals due to its slow diffusivity in the residual amorphous matrix. On the other hand, partial substitution of Ge for B in $Fe_{80}B_{20}$ amorphous alloy yields an increase of the Curie temperature and the magnetic moment [8]. In this work, $Fe_{75}Ge_xB_{20-x}Nb_5$ (x=0, 10 and 20 at. %) alloys were produced by mechanical alloying starting from powders of pure elements. Microstructure and magnetic properties were characterized and correlated. Nb was added in order to stabilize the nanocrystalline microstructure, acting as an inhibitor of the grain growth as it occurs in nanocrystalline microstructures achieved from PCPA. Also a study of the B/Ge ratio in the alloy is undertaken in this paper.

2. Experimental

$Fe_{75}Ge_xB_{20-x}Nb_5$ compositions (x=0, 10 and 20; in the following B, Ge-B and Ge alloys, respectively) were prepared from pure powders (purity≥99.85 %) by ball milling in a Retsch PM4000 planetary ball mill using hardened steel balls (10 mm diameter) and bowls. The initial powder mass was 30 g and the ball to powder ratio 12:1. Three continuous steps of 50 h, milling at 150 rpm, were performed, taking out some powder and the corresponding number of balls to keep constant the ball to powder ratio. The opening and closing of the bowls were done into a MBraun glove chamber in argon atmosphere to avoid oxygen and humidity contamination.

Size and morphology of the powder particles were studied by scanning electron microscopy (SEM) in a Philips XL-30. The microstructure of the powder was analyzed by X-ray diffraction (XRD) using Co-Kα radiation in a Philips PW1050 diffractometer and by Mössbauer spectrometry. Mössbauer spectra were recorded at room temperature in a transmission geometry using a ^{57}Co(Rh) source. Values of the hyperfine parameters

were obtained by fitting with NORMOS program [9]. The isomer shift, *I*, was quoted relative to that of α-Fe at room temperature. Thermal stability of the samples was studied by differential scanning calorimetry (DSC) using a Netzsch DSC-404C filling the chamber with argon after evacuating the air. This equipment was also used to heat the powder samples up to 773 and 1073 K. The magnetic transitions were detected by thermomagnetic gravimetry (TMG) in a Perkin-Elmer TGA7 thermobalance from the change of the apparent weight of the sample with the temperature applying a magnetic field of ~20 mT, under argon flow. In the absence of field, real weight changes were observed at high temperature, which allow the detection of the oxidation process. In the studied cases, this process is enhanced due to the large surface area of the studied samples as it will be shown below. Saturation magnetization, M_S, at 0.5 T was measured in a Lakeshore 7407 vibrating sample magnetometer (VSM). Coercivity, H_C, was measured using a Förster koerzimat.

3. Results

3.1 Scanning electron microscopy

Figure 1 shows SEM images of the different samples obtained after milling. As XRD results will show later, the main phase present in the powder particles is crystalline α-Fe type phase. The average particle size, *d*, was obtained from a statistical set of ~100 particles on each SEM pictures. From the point of view of powder morphology, after 50 h milling, B alloy does not show significant changes: 10.0 ± 0.8 μm, independently of the milling time. However, for Ge and Ge-B alloys, a clear increase of the average particle size is observed from 50 to 150 h milling (from 8.3 to 12.1 μm and from 8.0 to 21.8 μm for Ge-B and Ge alloys respectively) and the sphericity of the particles is enhanced as milling time increases. Particle size

distributions of the powder samples milled during 150 h are included in figure 1. The mean particle size increases with the Ge content in the alloy after 150 h milling (see above) as the broadening of the distribution does (standard deviations of the distributions are: 5, 6 and 8 μm for B, Ge-B and Ge alloys, respectively). It is worth noting that this average value represents the average size of the powder particles. However, it would be possible that some property depending on the powder particle size were dependent on the number of atoms contributing to such property. In such a case, the average powder particle size obtained is not representative and a volume weighted average powder particle size, d_V, must be defined as:

$$d_V = \frac{\sum_{i=1}^{N} d_i \cdot V_i}{\sum_{i=1}^{N} V_i} = \frac{\sum_{i=1}^{N} d_i^{\,4}}{\sum_{i=1}^{N} d_i^{\,3}} \qquad (1)$$

where V_i is the volume of the particle i and d_i is its size.

As an example, the importance of considering d_V instead of d has been shown in a study of the superparamagnetic behaviour of polydisperse systems [10]. In the present case, values of d_V after 150 h milling are 19.4, 20.4 and 27.9 μm for B, Ge-B and Ge alloys, respectively.

3.2 Differential scanning calorimetry

Figure 2 shows the DSC scans at 20 K/min of the three studied composition after milling during 150 h. A broad exothermic process is detected starting at ~550 K and extending up to 900-1000 K. This peak, characteristic of DSC scans of milled powder, is generally related to grain growth and stress relaxation phenomena [4]. For B alloy, a second exotherm is observed at ~880 K and a third one at ~1040 K, similar to that found for the studied Ge-B alloy. The last exothermic peak could be ascribed to the formation

of boride phases. This assumption is supported by the smaller enthalpy associated to this peak in Ge-B alloy and with its absence in the DSC scan of Ge alloy. A similar exotherm was also observed during the devitrification process of $Fe_{83-z}Nb_{10}Ge_zB_7$ (z=0, 3 and 10) [11]. In the case of Ge alloy, a sharp exotherm is found at 970 K. This peak could correspond to the formation of Ge rich phases and is absent in Ge-B alloy. The maximum solubility of Ge in the α-Fe lattice, 10 at. %, could yield the α-Fe,Ge phase of Ge alloy to be less stable than that of the Ge-B alloy. A DSC exotherm transformation was observed in the same temperature range for amorphous $Fe_{80}Nb_{10}Ge_3B_7$ [11] and ascribed to the formation of hexagonal Fe_3Ge phase.

3.3 X-ray diffraction

Figure 3 shows the XRD pattern of samples after milling during different times. A calculated XRD pattern of the initial powder is also shown for comparison as an approach to the XRD pattern of the mixed powder before milling. This pattern was calculated from the experimental ones of the pure elemental powders used, added after normalization, taking into account the atomic scattering factor values at 52º of the different elements and the composition of the alloy. It is worth noting the low scattering factor of the B atoms, which makes difficult to detect the contribution of this element. In all the studied cases, the main phase after milling is a bcc solid solution α-Fe type phase, independently of the time and composition. The asymmetric shape of the tail of the (110) diffraction maximum peaked at 2θ~52º indicates the presence of an amorphous halo centred at a lower value of 2θ. In the case of B alloy, a small extra peak at 2θ~43º is observed, possibly due to a boride phase developed during the milling process. For Ge containing alloys, no extra diffraction peaks appear after 150 h of milling, although for Ge alloy after 50 h milling, some residual peaks of initial Ge and

Intermetallics. Vol. 15. Núm. 10. 2007. Pag. 1351-1360
http://dx.doi.org/10.1016/j.intermet.2007.04.008

Nb phases are still present. The lattice parameter of the α-Fe type phase, *a*, was obtained from the position of the (110) and the (200) maxima. The lattice parameter of the α-Fe phase of B alloy (2.864±0.010 Å) is in agreement with the value of pure α-Fe (*a*=2.8665 Å). In the case of Ge containing alloys, the lattice parameter is clearly larger than that of B alloy (2.895 and 2.891±0.015 for Ge and Ge-B alloys respectively), in agreement with the effect of Ge in the lattice parameter of this phase [12,13,14]. The error bar does not allow to detect any difference between Ge-B alloy and Ge alloy (with twice the Ge content than that in Ge-B alloy), although the saturation value of Ge content inside the nanocrystals could be higher than 10 at. %, which is the maximum solubility of Ge in α-Fe [15].

In order to extract further information from the XRD pattern a single peak fitting procedure has been followed. Some reasons prevent us for using a whole profile fitting technique, very suitable when the identity (composition) of the present phases is well defined and they exhibit a high number of diffraction maxima (low symmetry crystal structure). In the studied case, the main phase is a bcc structure and, moreover, there is an amorphous phase which would modify the baseline of the pattern. On the other hand, small inhomogeneities in the powder composition would lead to a lattice parameter distribution of the bcc phase in the sample, which would produce a broadening of the maxima, increasing as the diffraction angle increases. Therefore, the diffraction maximum formed by overlapping of the (110) line of α-Fe phase and the main amorphous halo was chosen for a single peak fitting procedure as it is less affected by these effects. First, a deconvolution procedure for the (110) maximum and the amorphous halo was done to extract information of the nanocrystalline phase formed during milling. The amorphous halo was fitted by a Gaussian function, whereas a Pseudovoigt one was used to fit the crystalline peak. The area ratio of the (110)

maximum and the amorphous halo was used to estimate the crystalline volume fraction, *X*. A slightly larger value of *X* is found in the case of Ge containing alloys, which is in agreement with the detection of intermetallics in the XRD pattern of B alloy and with the fact that Ge is soluble in α-Fe phase while B is not. In fact, the amount of amorphous phase for Ge containing alloys is of the order of the error for these alloys (see table 1). Therefore, its quantification lacks of precision, although the asymmetry observed in the XRD peak evidences its existence.

The average grain size, <*D*>, was calculated from the broadening of the Lorentzian contribution to the Pseudovoigt fit to the (110) maximum, β_L, using Scherrer's formula:

$$< D >= \frac{0.9\lambda_{CoK\alpha}}{\beta_L \cos(\theta)} \tag{2}$$

where $\lambda_{CoK\alpha}$ is the wavelength of the Co Kα radiation. The microstrain, ε, was estimated from the broadening of the Gaussian contribution, β_G, as:

$$\varepsilon = \frac{\beta_G}{4\tan(\theta)} \tag{3}$$

In order to obtain the Gaussian (β_G) and Lorentzian (β_L) breadths, a single line method based on the shape factor of a Voigt function, ϕ, was used [16]. This factor is the ratio between the full width at half maximum (*FWHM*) and the integral broadening (β), which is the area divided by the intensity at the peak. This shape factor varies from 0.93949 (pure Gaussian) to 0.63662 (pure Lorentzian). Once the value of ϕ is known, the values of β_G and β_L can be obtained from the following empirical equations [16]:

$$\beta_G = \beta\left(0.6420 + 1.4187\sqrt{\phi - \frac{2}{\pi}} - 2.2043\phi + 1.8706\phi^2\right) \tag{4}$$

$$\beta_L = \beta\left(2.0207 - 0.4803\phi - 1.7746\phi^2\right) \tag{5}$$

The values of <*D*> and ε are similar for the three studied alloys (~5 nm and 1 %, respectively). These values agree with those found for the steady state of Fe-based alloys submitted to ball milling [4]. Results obtained are summarized in table 1.

The XRD data of samples milled 150 h and heated up to 773 and 1073 K are shown in figure 4 along with the corresponding XRD pattern of as-milled samples for the three studied alloys. Nanocrystalline microstructure remains after heating up to 773 K for all the studied compositions but after heating up to 1073 K this microstructure is not observed.

3.4 Mössbauer spectroscopy

Microstructure of as-milled powder was also analyzed using Mössbauer spectrometry. Figure 5 shows the Mössbauer spectra of the different as-milled samples. This technique has been shown as a powerful tool in determining the local arrangements in Fe containing alloys, supplying extra information from a different point of view, which can be correlated with that from other techniques as XRD. The main phase detected by XRD in the three studied alloys is α-Fe. The Fe atoms in pure α-Fe sites (surrounded by 8 Fe atoms as near neighbours, NN, and 6 Fe atoms as next near neighbours, NNN) must have a hyperfine field, *HF*=33 T. However, some lower *HF* values ascribed to atoms in crystalline positions can be found in an appreciable amount if the composition differs from that of pure Fe or if the size of the bcc crystallites is small enough to have a significant fraction of atoms in the surface of the crystal. Both effects would produce a different local configuration than that of the pure α-Fe in the inner region of the crystallite [17,18].

In the present study, the size of the nanocrystals is small enough, Ge is soluble in the α-Fe phase and mechanical alloying can induce the presence of elements inside the

Intermetallics. Vol. 15. Núm. 10. 2007. Pag. 1351-1360
http://dx.doi.org/10.1016/j.intermet.2007.04.008

nanocrystals, which would be absent if they were formed in equilibrium conditions (B and Nb). Therefore, in order to fit the spectra, a *HF*=33 T contribution has been imposed (characteristic of a pure α-Fe local environment) along with two *HF* distributions: one for high values of *HF*, ascribed to Fe atoms mostly surrounded by Fe (Fe atoms in α-Fe phase with Ge atoms as NN or at interface sites), and another one for low *HF* values, ascribed to Fe atoms surrounded by elements different to Fe (amorphous or intermetallic phases). The resultant distributions of hyperfine fields used in the fitting are shown in Figure 6. Due to the uncertainty of the limits of both distributions, some overlapping of them was allowed (low field distribution extends from 0 to 29 T and high field distribution extends from 21 to 35 T), and the discussion of Section 4 will consider the resultant distribution as a whole: total distribution will corresponds to the Mössbauer response of those atoms which are not in a pure α-Fe local enviroment. Table 2 shows the average values of isomer shift and hyperfine magnetic field obtained from the fitting.

3.5 Thermomagnetic gravimetry

Figure 7 shows the TMG heating and cooling cycles of samples milled during 150 h: heating up to 773 K, cooling down to room temperature and heating up again up to 1073 K. Samples milled during 50 and 100 h show no significant differences with respect to their corresponding 150 h milled ones. As-milled samples do not exhibit any Curie transformation below 773 K. However, the low field magnetization plot shows changes after this treatment. However, the applied field is low (~20 mT) to saturate the sample and the observed changes also can be due to stress relief and to some change in the demagnetization factor of the sample as the powder particles became stuck. At higher temperatures different Curie transitions are observed. The main fall in

magnetization in each case can be ascribed to the Curie transition of the α-Fe phase which is also the main phase observed by other techniques.

In every studied case, after the fall in magnetization due to the Curie transition of the α-Fe type phase, a zero value is not reached. The origin of this non-zero value is not magnetic but due to the oxidation of the samples. In fact, although TMG experiments were performed in argon flow, the powder was encapsulated in air into silver pans and the oxygen retained might remain during the experiment. This effect, always present in the experiments but negligible when pieces of ribbon are used [19], is extraordinarily enhanced for powder samples because of the large surface area of these systems. In order to demonstrate this, the experiment in the thermobalance was repeated in the same conditions but without applying any magnetic field. Figure 8 shows the apparent weight measured in both experiments with and without applied field for a powder sample of B alloy milled during 150 h. Oxidation is more important as Ge content increases in the alloy and, for the Ge alloy, it is evident even for samples heated only up to 773 K.

3.6 Saturation magnetization and coercivity.

Figure 9 shows the saturation magnetization, M_S, (at 0.5 T) and the coercivity, H_C, versus milling time for B and Ge alloys. B alloy shows no significant change in the powder particle size with the milling time and Ge alloy shows the largest differences between 50 and 150 h. Whereas M_S is almost independent of milling time (error bar 10 %), the coercivity decreases with milling time, being this effect larger for the Ge alloy.

Figure 10 shows M_S, the magnetic moment per Fe atom, μ_{Fe}, and H_C for the three studied composition milled 150 h, in the as-milled state and after heating up to 773 and 1073 K. Although neither M_S, nor μ_{Fe} show significant evolution with the

Intermetallics. Vol. 15. Núm. 10. 2007. Pag. 1351-1360
http://dx.doi.org/10.1016/j.intermet.2007.04.008

heating temperature, H_C decreases after heating up to 773 K to increase after heating up to 1073 K, independently of the studied alloy.

4 Discussion

4.1 Microstructure of as-milled samples

Mössbauer spectra and the *HF* distributions of as-milled B alloy samples are almost independent of milling time. Due to the milling process, some B and Nb atoms could be dissolved into the α-Fe phase. However, this effect should be small enough to be neglected (supported by the value of the lattice parameter of the B-alloy, which is independent of milling time and in agreement with that of pure α-Fe). Therefore, for this composition, 33 T contribution corresponds to pure α-Fe sites (inner regions of the nanocrystal), the *HF* contributions above ~20 T should be ascribed to Fe atoms at the interface and the peak at ~10 T to some intermetallic compound, which was also detected by XRD (as *HF*~12 T for FeB [20], this phase can be considered). The rest of the contributions could correspond to the residual amorphous phase (14-23 % of the total as can be seen in table 1). The crystal size can be estimated from the relative fraction of atoms at interface sites and at crystalline sites using:

$$D = 2\delta \frac{\sqrt[3]{\frac{A_I}{A_C}+1}}{\sqrt[3]{\frac{A_I}{A_C}+1}-1} \qquad (7)$$

where A_I is the fraction of Fe atoms at the interface and A_C is the fraction of Fe atoms in the inner regions of the nanocrystal obtained from Mössbauer results. For B alloy, ascribing the high field region, ≥20 T, to interface sites and considering the thickness of the interface δ~0.5 nm [21], a grain size of 4.5±0.5 nm is obtained, independently of milling time and in agreement with the results obtained from XRD (~5 nm).

Intermetallics. Vol. 15. Núm. 10. 2007. Pag. 1351-1360
http://dx.doi.org/10.1016/j.intermet.2007.04.008

Unlike B alloy, Mössbauer spectra of Ge containing alloys show a clear evolution with milling time, not observed by XRD. For these alloys, it is worth noting the presence in the Mössbauer spectra of a sharp peak slightly below 6 mm/s (ascribed to the 33 T contribution of pure α-Fe local enviroment), which decreases as milling time increases but remains even after 150 h. These peaks are observed in the experimental data of the Mössbauer spectra of Fig. 5 and at 33 T in the *HF* distributions of Fig. 6. They indicate the existence of local pure α-Fe enviroments in a higher concentration than that expected for a homogeneous solid solution of α-Fe,Ge disordered phase, for which a smooth shape of the *HF* distribution is expected. This could be explained assuming the existence of two different α-Fe type phases: one close to pure Fe and another with Ge, which grows as milling time increases. However, XRD data do not show the presence of two bcc lattices but only one with a lattice parameter almost constant and clearly larger than that of the pure α-Fe. Nevertheless, a discrete 33 T contribution is evident in the *HF* distribution, at least for 50 h of milling. Therefore, this fact could be ascribed to some degree of ordering (DO3 or B2), which decreases as milling time increases. In fact, it has been shown that ordering clearly affects the hyperfine field distribution in Fe-base alloys and could yield to the appearance of discrete *HF* contributions for single phases [22,23]. It is worth noting that, if iron-rich inhomogeneities were responsible for the sharp 33 T contribution, the crystal size obtained from XRD would be underestimated. In the case of Ge containing alloys, unlike B alloy, the high fields below 33 T are ascribed not only to interface sites but also to the presence of Ge as NN and NNN in the α-Fe lattice. The extra peak observed for B alloy at ~10 T was not observed in the *HF* distributions of Ge containing alloys, in agreement with the absence of the boride phase in XRD results, but a single broad maximum to which the 33 T contribution is superimposed. Therefore, only crystalline,

interface and amorphous Fe sites can be considered in the *HF* distribution in alloys with Ge. This broad maximum is more extended to low *HF* values for Ge alloy than for Ge-B alloy, indicating a higher concentration of Ge in the crystals for the former composition. Considering only the first shell around a Fe atom, the *HF* values corresponding to 1, 2, 3 and 4 Ge atoms as NN are approximately 33, 29, 24 and 20 T, respectively [12]. In particular, the contribution at 20 T is clear for Ge alloy but less evident for Ge-B alloy (see Fig. 6) taking into account that the interface sites might contribute too.

4.2 Phase identification of annealed powders

Two annealed samples (heated up to 773 and 1073 K, respectively) were prepared from each alloy milled during 150 h. XRD patterns of figure 4 show that samples heated up to 773 K remain in the nanocrystalline state, without a significant change neither in the crystalline volume fraction nor in the crystal size (5, 5 and 6 nm for B, GeB and Ge-alloy respectively) or in the lattice parameter. However, microstrain decreases down to 0.5 %, indicating that the very broad exotherm is mainly related to stress relaxation processes. Some small intensity peaks are observed in the Ge alloy heated up to 773 K, which correspond to the DO3 ordered fcc-Fe_3Ge phase.

Heating up to 1073 K leads to fully crystalline samples. In Ge alloy, the DO3 phase becomes more evident and coexists with the hexagonal Fe_3Ge phase. Several phases could be ascribed to the peaks observed for the XRD pattern of the B-alloy heated up to 1073 K: FeB, $Fe_{23}B_6$, FeNb and FeNbB.

Samples heated up to 773 K show a reversible TMG behaviour up to this temperature and a clear fall in magnetization associated to the Curie transition of the α-Fe phase. This fall is double in Ge containing alloys (~780 and 830 K for Ge alloy, and 830 and 1000 K for Ge-B alloy, as it is shown in the insets of Fig. 7) but single in B

alloy (1036 K). In the case of Ge-alloy, the first fall is not observed after heating the sample up to 1073 K. This indicates that the Curie transition at ~780 K would correspond to a metastable phase, probably an extended solid solution of α-Fe,Ge, as no other phase is observed by XRD neither for the as-milled sample nor for the sample heated up to 773 K. Amorphous phase is discarded due to its small volume fraction (see table 1). The second Curie transition remains after heating up to 1073 K, which indicates a higher thermal stability of this α-Fe,Ge phase. However, its Curie temperature, 830 K, is much lower than that corresponding to the maximum solubility of Ge (10 at. % [15]) in α-Fe or ordered fcc-Fe_3Ge, indicating the existence of an extended solid solution that remains stable at these temperatures. In the case of Ge-B alloy, the first fall at 830 K remains after heating the sample up to 1073 K. Therefore, the corresponding phase could be that ascribed to the second transformation of Ge-alloy, as the Curie temperatures are coincident. However, it could also correspond to the Curie transition of some oxide, as it is explained below. The second fall in magnetization, at 993 K, is slightly lower than that corresponding to 10 at. % of Ge in α-Fe phase [15]. The single Curie transition observed for B alloy, 1036 K, is very close to that of pure α-Fe. However, for this alloy, XRD and Mössbauer data showed the presence of FeB ferromagnetic intermetallic in the as-milled state. The Curie temperature of this phase is ~600 K [8,24]. Relaxation process affects the TMG signal of the as-milled sample in this temperature range and could prevent a clear detection of this Curie transition but, after heating up to 773 K, a very faint maximum could be observed at ~610 K in the derivative of the magnetization, independently of milling time, which roughly agrees with the expected value.

After heating the samples up to 1073 K, the final cooling curve shows the Curie transition of the magnetic phases present in the fully crystalline sample (Fig. 7). In the

case of B alloy, along with the Curie transition of the α-Fe phase, another one at ~845 K appears. This is not coincident with any value of Fe boride phase [24] but a good agreement with *magnetite* Fe_3O_4 oxide is found [25]. For Ge-B alloy, besides the α-Fe,Ge (Ge content slightly above 10 at. %) and Fe_3O_4 Curie transitions, a new one appears at ~473 K, which could correspond to hexagonal Fe_3Ge_2 phase (with large compositional variability, e.g. Fe_3Ge) [26]. In Ge alloy, besides the Curie transition of α-Fe,Ge/fcc Fe_3Ge phase (~845 K, possibly overlapped with the transition of Fe_3O_4) and that of the hexagonal Fe_3Ge phase, a weak transition is detected at ~630 K, which could be ascribed to some Ge containing Fe oxide, as the Fe_2GeO_4 spinel (*Brunogeierite*, coherent with XRD results [27]), although no Curie temperature data could be found in the literature for this or similar compounds. The agreement between XRD and TMG data supports the phase identification performed.

4.3 Relationship between microstructure and magnetic properties

The decrease of the coercivity of as-milled samples shown in Fig. 9 is correlated with the increase in powder particle size observed by SEM as milling time increases (see inset of Fig. 9). This effect is stronger in Ge alloy than in the other studied compositions, in agreement with SEM results, which show an important change in the powder particle size. As the powder particle increases, being multidomain systems, the movement of the magnetic domain walls would become easier and the material would become magnetically softer. Another possible effect was pointed by Chicinas et al [28], who linked the coercivity of Fe powder with the particle size, ascribing the magnetic softening to the decrease of the residual stresses as the particle size increases. On the other hand, Shen et al [5] found that the dislocation density is the main parameter

affecting the coercivity. The error bar in the estimation of microstrain by XRD results prevents further discussion of this point in the present study.

After heating up to 773 K, coercivity decreases due to the release of internal stresses. The lowest value was found for Ge alloy heated up to 773 K, with H_C~600 A/m, a fairly good value for a powder sample [5] and promising to deserve further studies. This stronger reduction compared with that of B or GeB alloys could be due not only to stress release but also to some ordering of bcc α-Fe,Ge phase towards the ordered fcc Fe_3Ge, as it was observed by XRD. Finally, for samples heated up to 1073 K, coercivity increases again due to the formation of intermetallic compounds, being the hardening larger in B alloy. Annealing does not significantly change M_S but there are some differences for the three compositions studied. However, most of this difference is due to the different density of Ge and B. If μ_{Fe} is considered, all compositions exhibit a similar value, slightly below 2 μ_B.

4. Conclusions

Microstructure, thermal stability and magnetic properties of three Fe-Nb-(B,Ge) alloys have been studied. The main conclusions are listed below.

- XRD and Mössbauer results agree describing a nanocrystalline microstructure (~5 nm in size) and the existence of a small amount of amorphous phase. This amorphous phase is ~20 % in the case of Fe-B-Nb alloy.
- Intermetallics are formed in Fe-B-Nb system but they were not detected by XRD in Fe-Ge-(B)-Nb systems after 150 h milling. For Ge containing alloys, some traces of Nb and Ge remains after 50 h of milling.

- In Fe-B-Nb alloy, Mössbauer spectrometry shows no evolution of the α-Fe phase formed from 50 to 150 h milling. However, Fe-Ge-(B)-Nb alloys evolve, decreasing the contribution of the pure α-Fe sites.
- The decrease in coercivity of as-milled samples with the increase of the milling time is ascribed to the increase in powder particle size observed by SEM.
- The decrease in coercivity for samples heated up to 773 K with respect to as-milled samples is related to stress relaxation (a microstrain reduction was observed from XRD). The large decrease in Fe-Ge-Nb could be ascribed to some ordering of the α-Fe(Ge) phase in fcc Fe_3Ge phase.

Acknowledgments

This work was supported by the Spanish Government and EU FEDER (Project MAT 2004-04618) and by the PAI of the Regional Government of Andalucía (Spain). J.S.B. acknowledges a research contract from this Regional Government.

Intermetallics. Vol. 15. Núm. 10. 2007. Pag. 1351-1360
http://dx.doi.org/10.1016/j.intermet.2007.04.008

References

[1] Y. Yoshizawa Y, Oguma S, Kamauchi K, J Appl Phys 1988; 64: 6044.

[2] McHenry ME, Willard MA, Laughlin DE, Prog Mater Sci 1999; 44: 291.

[3] Skorvanek I, Svec P, Greneche JM, Kovac J, Marcin J, Gerling R, J Phys: Condens Matter 2002; 14: 4717.

[4] Suryanarayana C, Prog Mat Sci 2001; 46: 1.

[5] Shen T, Schwarz RB, Thompson JD, Phys Rev B 2005; 72: 014431.

[6] Stoica M, Roth S, Eckert J, Schultz L, Baró MD, J Magn Magn Mat 2005; 290-291: 1480.

[7] Suzuki K, Makino A, Kataoka N, Inoue A, Masumoto T, Mater Trans JIM 1991; 32: 93.

[8] Soshow KN, Masumoto T, Mitera M, J Magn Magn Mat 1980; 15-18: 1331.

[9] Brand RA, Lauer J and Herlach DM, J Phys F: Met Phys 1983; 13: 675.

[10] Blázquez JS, Franco V, Conde CF, Conde A, J Nanosci Nanotech 2007; 7: 1043.

[11] Mao X, Han Z, Xu F, Gao W, Gu B, Du Y, Appl Phys A 2005; 81: 839.

[12] Kwon YS, Gerasimov KB, Lomovsky OI, Pavlov SV, J All Compd 2003; 353: 194.

[13] Cabrera AF, Sánchez FH, Phys Rev B 2002; 65: 094202.

[14] Konygin GN, Yelsukov EP, Porsev VE, J Magn Magn Mat 2005: 288; 27.

[15] Massalski TB, Okamoto H, Subramanian PR, Kacprzak L. Binary Alloys Phase Diagrams. Materials Park, Ohio: ASM International, 1992. p. 1187, 1706.

[16] Keijser ThH, Langford JI, Mittemeijer EJ, Vogels ABP, J Appl Cryst 1982; 15: 308.

[17] Wertheim GK, Jaccarino V, Wernick JH, Buchanan DNE, Phys Rev Letters 1964; 12: 24.

[18] Miglierini M, Grenèche JM, J Phys: Condens Matter 1997; 9: 2321.

[19] Borrego JM, Conde CF, Conde A, Phil Mag Letters 2000; 80: 359.

[20] Murphy KA, Hershkowitz N, Phys Rev B 1973; 7: 23.

[21] Blázquez JS, Franco V, Conde A, J All Compd 2006; 422: 32.

[22] Borrego JM, Blázquez JS, Conde CF, Conde A, Roth S, Intermetallics 2007; 15: 193.

[23] Blázquez JS, Conde A, Grenèche JM, J Phys: Cond Matter 2003; 15: 7843.

[24] Chien CL, Unruh KM, Phys Rev B 1984; 29: 207.

[25] Smith DO, Phys Rev 1956; 102: 959.

[26] Albertini F, Pareti L, Deriu A, Negri D, Calestani G, Moze O, Kennedy SJ, Sonntag R, J Appl Phys 1998; 84: 401.

[27] Welch MD, Cooper MA, Hawthorne FC, Mineralogical Mag 2001; 65: 441.

[28] Chicinas I, Jumate N, Matei Gh, J Magn Magn Mat 1995; 140-144: 1875.

Intermetallics. Vol. 15. Núm. 10. 2007. Pag. 1351-1360
http://dx.doi.org/10.1016/j.intermet.2007.04.008

Figure captions

Figure 1. SEM images of different as-milled samples. Particle size distributions of samples after 150 h milling are shown below for each composition. Magnification is the same for all the images.

Figure 2. DSC scans of powder after 150 h of milling. Arrows indicate the temperatures at which samples were heated for microstructural and magnetic characterization.

Figure 3. XRD patterns of as-milled samples. The calculated XRD patterns of the initial powder mixtures are shown above for comparison.

Figure 4. XRD of as-milled and thermally treated samples.

Figure 5. Mössbauer spectra of as-milled samples. Experimental data are represented by circles, thick lines correspond to the total fitting and thin lines correspond to each contribution used in the fitting (see text).

Figure 6. Total HF distribution of as-milled samples. Note the breaks in the Y axis where applicable.

Figure 7. TMG heating and cooling cycles for samples milled during 150 h. Arrows indicate the sense of the curve (heating or cooling) and numbers correspond to: 1, as-milled sample; 2, samples heated up to 773 K; and 3, samples heated up to 1073 K. The ellipses indicate the regions enlarged in the corresponding insets. In Ge-alloy, this enlargement is used to clarify the crossing between 2 and 3 curves. In GeB-alloy, it is also shown to appreciate the small Curie transition at 830 K after heating the sample up to 773 K.

Figure 8. TMG (applying a magnetic field of ~20 mT) and TG (zero field applied) plots of $Fe_{75}B_{20}Nb_5$ alloy after milling during 150 h.

Figure 9. Magnetization at 0.5 T and coercivity versus milling time. Lines are a guide to the eye.

Intermetallics. Vol. 15. Núm. 10. 2007. Pag. 1351-1360
http://dx.doi.org/10.1016/j.intermet.2007.04.008

Figure 10. Magnetic moment per Fe, magnetization at 0.5 T and coercivity versus temperature of treatment, T_{heat}. Lines are a guide to the eye.

Intermetallics. Vol. 15. Núm. 10. 2007. Pag. 1351-1360
http://dx.doi.org/10.1016/j.intermet.2007.04.008

Table 1. Results on microstructure of as-milled powder samples. <*d*>, mean powder particle size; σ, standard deviation; <d_V>, volume weight average powder particle size; <*D*>, average crystal size; ε, average microstrain; *X*, crystalline volume fraction; *a*, lattice parameter of α-Fe phase.

Alloy	Milling time (h)	<*d*> ±0.4 (μm)	σ (μm)	<d_V> ±5 (μm)	<*D*> ±2 (nm)	ε ±0.5 (%)	*X* ±10 (%)	*a* ±0.01 (Å)
B	50	9.6	5.3	20	5	1.0	0.86	2.86
	100	9.2	4.9	18	5	0.8	0.80	2.85
	150	11.1	5.4	19	6	1.0	0.77	2.87
Ge-B	50	8.3	4.5	14	7	1.2	0.94	2.89
	100	10.0	5.6	18	5	0.9	0.95	2.89
	150	12.1	6.0	20	5	1.1	0.95	2.89
Ge	50	8.0	3.4	12	7	1.6	0.89	2.87
	100	10.7	5.3	18	4	1.1	0.90	2.88
	150	21.8	7.8	28	5	1.1	0.93	2.90

Intermetallics. Vol. 15. Núm. 10. 2007. Pag. 1351-1360
http://dx.doi.org/10.1016/j.intermet.2007.04.008

Table 2. Mössbauer results. <*I*>, average isomer shift; <*HF*>, average magnetic hyperfine field.

Alloy	Milling time (h)	<*I*> ±0.01 (mm/s)	<*HF*> ±0.5 (T)
B	50	0.02	26.5
	100	0.02	26.6
	150	0.02	26.2
Ge-B	50	0.08	28.7
	100	0.10	27.1
	150	0.10	26.8
Ge	50	0.16	26.1
	100	0.18	24.9
	150	0.18	24.9

Intermetallics. Vol. 15. Núm. 10. 2007. Pag. 1351-1360
http://dx.doi.org/10.1016/j.intermet.2007.04.008

Figure 1

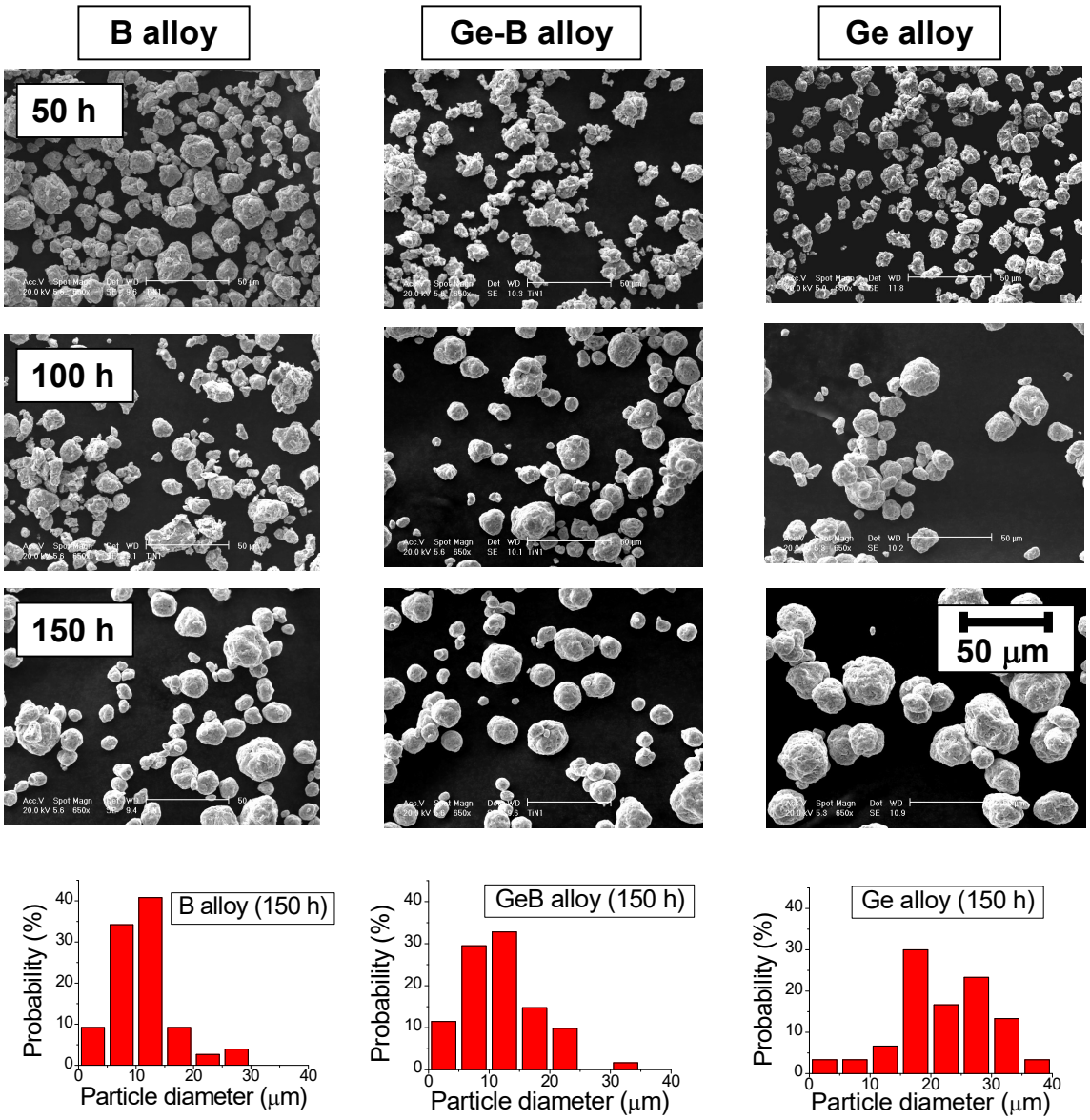

Intermetallics. Vol. 15. Núm. 10. 2007. Pag. 1351-1360
http://dx.doi.org/10.1016/j.intermet.2007.04.008

Figure 2

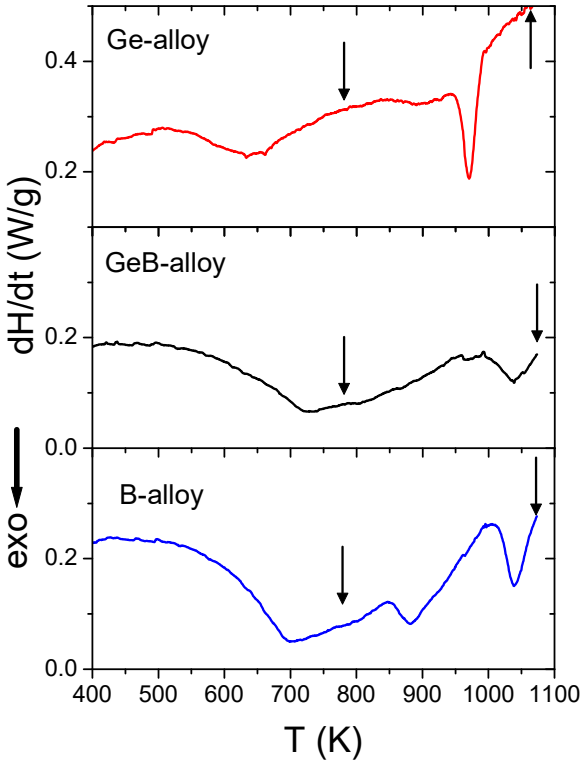

Intermetallics. Vol. 15. Núm. 10. 2007. Pag. 1351-1360
http://dx.doi.org/10.1016/j.intermet.2007.04.008

Figure 3

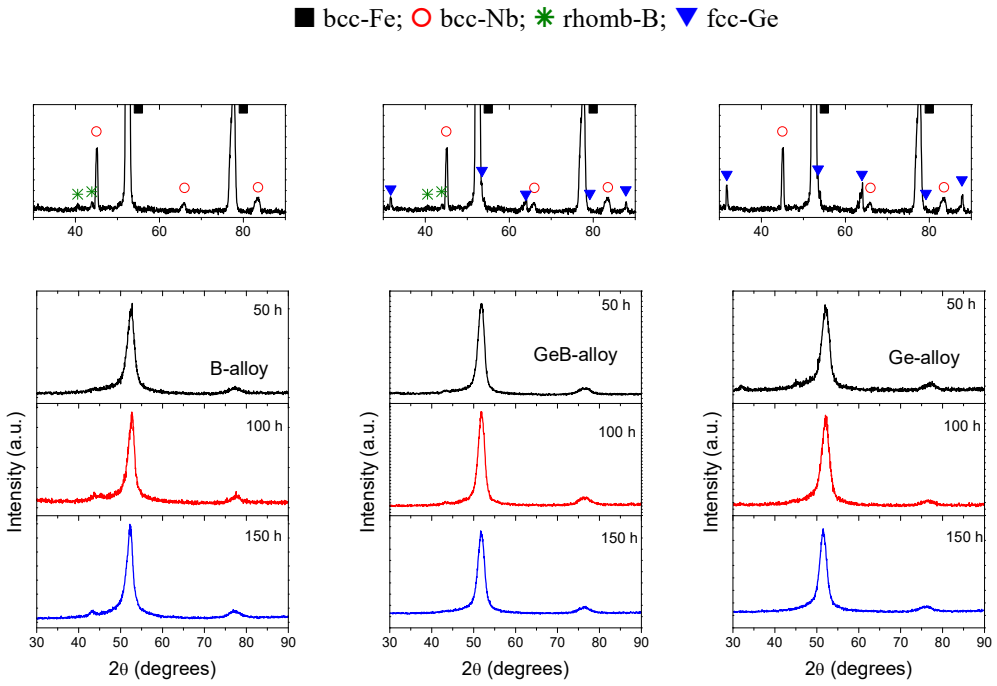

Intermetallics. Vol. 15. Núm. 10. 2007. Pag. 1351-1360
http://dx.doi.org/10.1016/j.intermet.2007.04.008

Figure 4

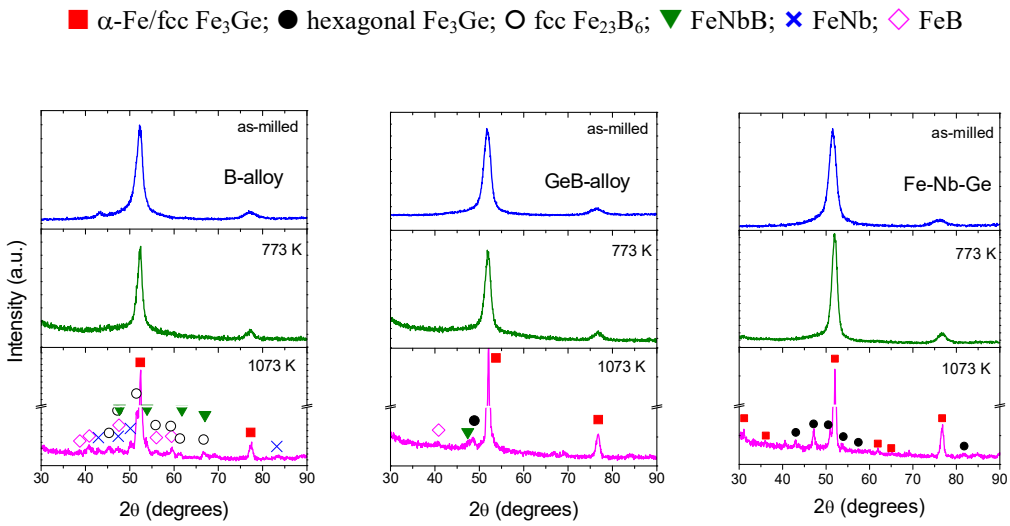

Intermetallics. Vol. 15. Núm. 10. 2007. Pag. 1351-1360
http://dx.doi.org/10.1016/j.intermet.2007.04.008

Figure 5

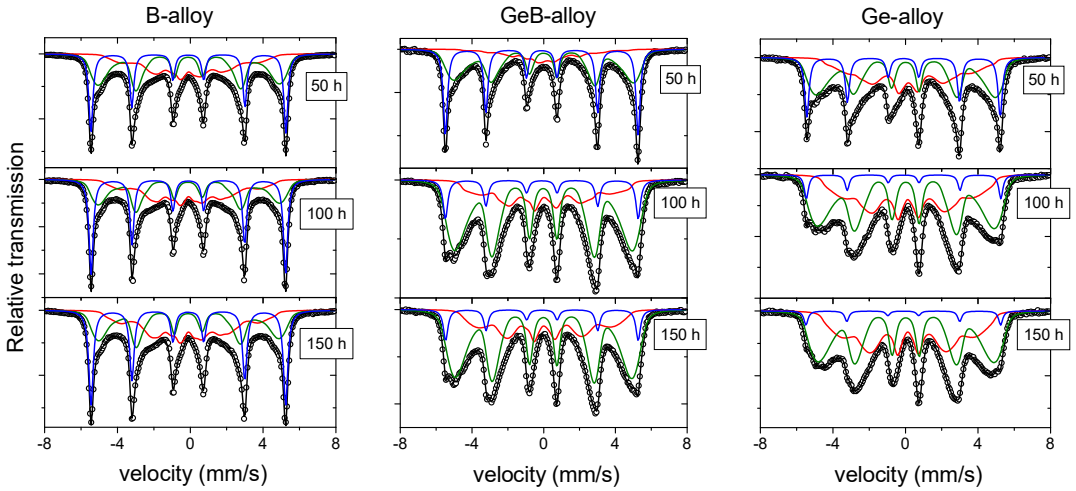

Intermetallics. Vol. 15. Núm. 10. 2007. Pag. 1351-1360
http://dx.doi.org/10.1016/j.intermet.2007.04.008

Figure 6

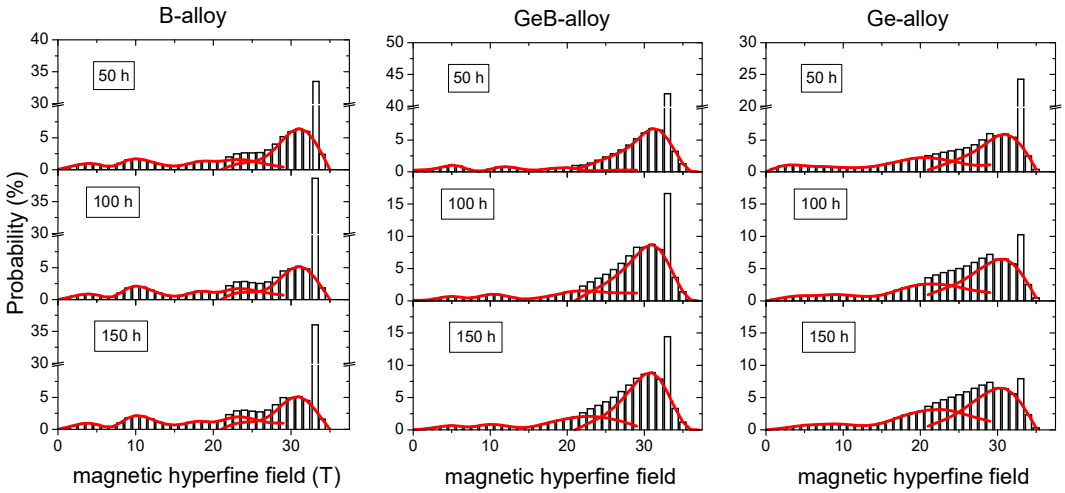

Intermetallics. Vol. 15. Núm. 10. 2007. Pag. 1351-1360
http://dx.doi.org/10.1016/j.intermet.2007.04.008

Figure 7

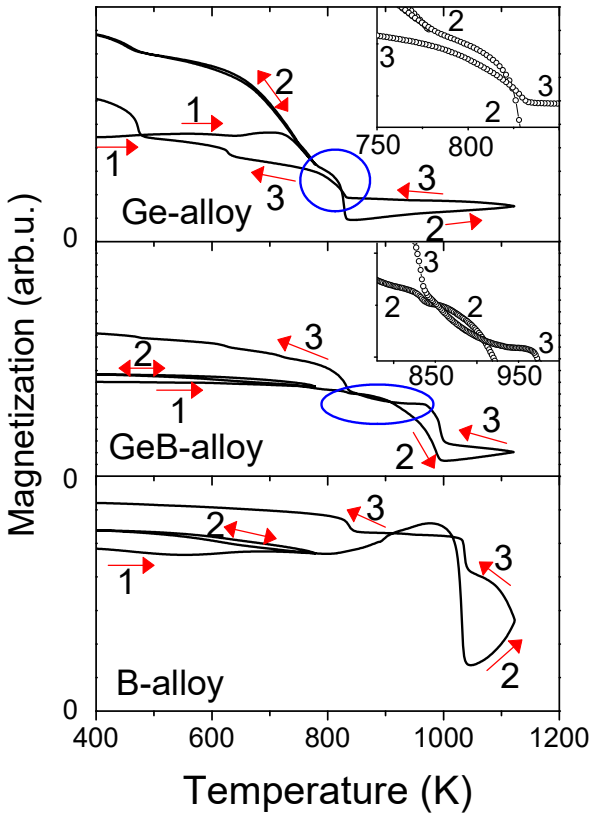

Intermetallics. Vol. 15. Núm. 10. 2007. Pag. 1351-1360
http://dx.doi.org/10.1016/j.intermet.2007.04.008

Figure 8

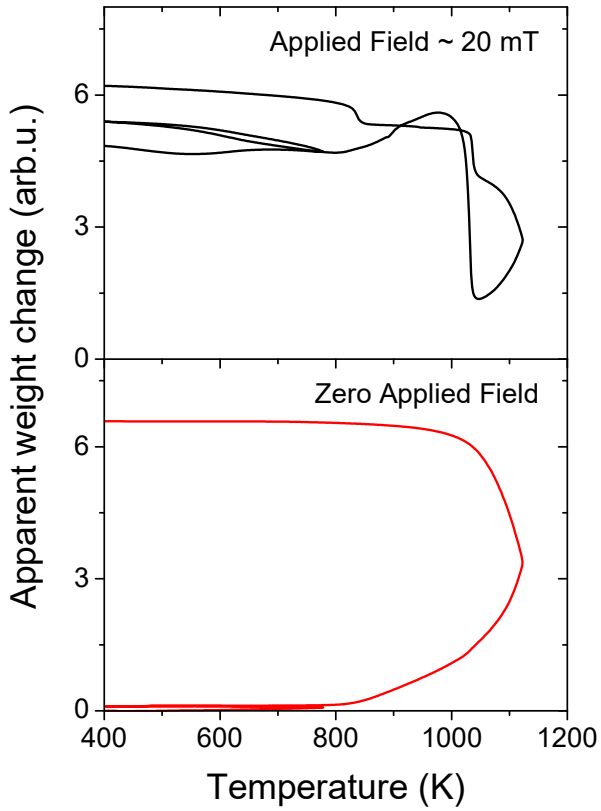

Intermetallics. Vol. 15. Núm. 10. 2007. Pag. 1351-1360
http://dx.doi.org/10.1016/j.intermet.2007.04.008

Figure 9

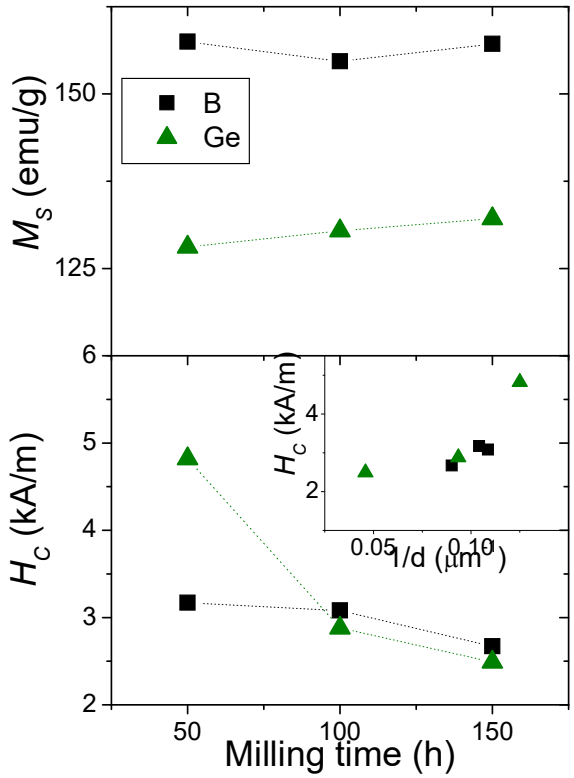

Intermetallics. Vol. 15. Núm. 10. 2007. Pag. 1351-1360
http://dx.doi.org/10.1016/j.intermet.2007.04.008

Figure 10